

Article

Effect of Nanofluid Thermophysical Properties on the Performance Prediction of Single-Phase Natural Circulation Loops

Nur Çobanoğlu¹ and Ziya Haktan Karadeniz^{2,*} ¹ Graduate School of Natural and Applied Sciences, İzmir Kâtip Çelebi University, 35620 İzmir, Turkey; ncobanoglu93.phd@gmail.com² Department of Mechanical Engineering, İzmir Kâtip Çelebi University, 35620 İzmir, Turkey

* Correspondence: zhaktan.karadeniz@ikcu.edu.tr

Received: 8 April 2020; Accepted: 11 May 2020; Published: 15 May 2020



Abstract: Specifying nanofluids' thermophysical properties correctly is crucial for correct interpretation of a system's thermo-hydraulic performance and faster market-uptake of nanofluids. Although, experimental and theoretical studies have been conducted on nanofluids' thermophysical properties; their order-of-magnitude change is still a matter of debate. This numerical study aims to reveal the sensitivity of single phase natural circulation loops (SPNCL), which are the passive systems widely used in solar thermal and nuclear applications, to thermophysical property inputs by evaluating the effects of measured and predicted nanofluid thermophysical properties on the SPNCL characteristics and performance for the first time. Performance and characteristics of an SPNCL working with water-based- Al_2O_3 nanofluid (1–3 vol.%) for heating applications is evaluated for different pipe diameters (3–6 mm). The thermal conductivity effect on SPNCL characteristics is found to be limited. However, viscosity affects the SPNCL characteristics significantly for the investigated cases. In this study, Gr_m ranges are 1.93×10^7 – 9.45×10^8 for measured thermophysical properties and 1.93×10^7 – 9.45×10^8 for predicted thermophysical properties. Thermo-hydraulic performance is evaluated by dimensionless heat transfer coefficients which is predicted within an error band of $\pm 7\%$ for both the predicted and measured thermophysical properties of the data. A Nu correlation is introduced for the investigated SPNCL model, which is useful for implementing the SPNCL into a thermal system.

Keywords: thermal conductivity; viscosity; nanofluid; single phase natural circulation loop; Nu correlation

1. Introduction

In a general sense, an increase in thermal conductivity by addition of nanoparticles into a base fluid (distilled water (DIW), ethylene glycol (EG), etc.), producing a nanofluid, results in higher heat transfer performance. Enhanced thermal conductivity is the main reason for the improved heat transfer performance, but the change in other thermophysical properties (especially viscosity) may reduce the overall efficiency of the system. Therefore, the correct interpretation of the convective heat transfer and overall efficiency is crucial for nanofluid applications to obtain a realistic conclusion [1,2].

The measurement of the thermophysical properties of nanofluids involves some difficulties due to the complex physical interaction between fluid and nano-particles [3]. The thermal conductivity and viscosity of nanofluids are the most studied properties since they highly influence the performance of the system [4–10]. Flow type and drag type viscometers are generally used for viscosity measurements and transient techniques, such as transient hot wire (THW) and 3- ω method, and are widely used to measure the thermal conductivity of nanofluids [3]. Measurements by commercial devices that are tuned for

ordinary fluids results in less accurate and/or misleading property values for nanofluids [11,12]. For example, Antoniadis et al. [11] published the necessary conditions for accurate transient hot wire measurements of nanofluid thermal conductivity. Non-standardized production and measurement procedures of nanofluids also introduced confusing empirical thermophysical property models, which are vital for the implementation of nanofluids into real-life applications for faster and cheaper design of engineering systems [13]. The accuracy of such models is improved by introducing parameters such as concentration, size and shape of particles, micro and nanoscale physical interactions, etc. [14,15]. Maxwell and Hamilton–Crosser, and Einstein and Brinkman models are widely used for thermal conductivity and viscosity prediction, respectively. The difference between Measured Thermophysical Properties (MTP) and Predicted Thermophysical Properties (PTP) by existing models has been studied widely. Table 1 presents a comparison of the data obtained from predictions and measurements for selected studies. It is seen that different models could give different results compared to each other and measurements for a nanofluid.

Table 1. Comparison of nanofluids’ thermophysical properties obtained from predictions and measurements for selected studies.

Ref.	Nanofluid	Measurement Method	Models	Comparison of Results
[16]	Al ₂ O ₃ -DIW (Ø10 and 30 nm) 1, 2, 3 and 6.33 vol.%,	Thermal conductivity: 3- ω method Viscosity: Brookfield Rheometer	Thermal conductivity: Maxwell model [17] Viscosity: Einstein model [18], Nguyen [19], Williams [20] and Chandrasekar [21]	Thermal conductivity: Measured values are comparable with the model Viscosity: Measured values are higher for Einstein, Nguyen, and Chandrasekar models but lower for the Williams model
[22]	TiO ₂ -DIW 0.5–5 vol.% Rod shape: Ø10 nm × 40 nm Spherical shape: Ø15 nm	Thermal conductivity: THW method	Thermal conductivity: Maxwell [17], Hamilton–Crosser [23] and Bruggeman [24] models	Thermal conductivity: Measured values are remarkably higher compared to the models
[25]	γ -Al ₂ O ₃ -DIW (Ø13 nm) and TiO ₂ -DIW (Ø27 nm) 0–10 vol.%	Viscosity: Brookfield Rheometer	Viscosity: Batchelor model [26]	Viscosity: Measured values are higher compared to the model
[27]	Fe-DIW (Ø37, 71 and 98 nm) 0.0313–1 vol.%	Thermal conductivity: THW method Viscosity: No information	Thermal conductivity: Hamilton–Crosser [23] and Yu and Choi [28] model Viscosity: Einstein [18] and Wang [29] models	Thermal conductivity: Measured values higher than models especially for >0.4 vol.% Viscosity: Measured values are higher than the Einstein model and lower than the Wang model
[30]	ZnO-EG (Ø18 nm) 0.25–5 vol.%	Viscosity: Brookfield Rheometer	Viscosity: Einstein [18], Batchelor [26] and Wang [29] models	Viscosity: Measured values are higher than the Einstein and Batchelor models and lower than the Wang model
[31]	Ag-DIW (Ø60 nm) 0.3–0.9 vol.%	Thermal conductivity: THW method Viscosity: Cannon–Fenske Viscometer	Thermal conductivity: Hamilton–Crosser [23], Timofeeva [32] and Wasp [33] models Viscosity: Einstein [18], Wang [29] and Brinkman [34] models	Measured values of both thermal conductivity and viscosity is higher than the existing models

Nanofluids have been implemented mostly in forced convection applications such as heat exchangers [35,36], pool boiling [37], solar thermal systems [38–45], cooling applications [46,47], etc. However, recent studies have shown that nanofluids have great potential in passive heat transfer systems where there is no pump-driven motion of the liquid [1].

Natural circulation loops (NCLs) are well-known passive components in heat transfer systems. NCLs have been used for many applications such as cooling of nuclear reactors, solar water heaters and electronic chip cooling [48–50]. Their reliability, stability and performance are widely studied [51–55]. In nuclear reactors, decay heat and core heat removal are provided by using NCL [50,51,56,57]. NCLs

are also getting attention for solar thermal applications. Utilization of NCL in solar water heating system avoids freezing and corrosion problems and nighttime heat losses [58], and when a solar still system is designed as NCL, water vapor is transferred from evaporator to condenser without direct contact [59,60]. Moreover, Michael and Iniyan [61] compared the performance of CuO/DIW nanofluid in a flat plate solar water heater under natural and forced circulations. Although the highest efficiency is observed for forced circulation, they found that the highest efficiency improvement occurs for natural circulation.

In single phase natural circulation loops (SPNCLs), temperature difference causes a density gradient (without phase change) and resulting buoyancy forces are the driving mechanism of SPNCLs. They are getting attention due to their advantages of simplicity, easy control, enhanced safety and reliability. In order to obtain a high-performance SPNCL together with robust characteristics (i.e., highly efficient heat transfer and stable flow) within a desired operational range, the effect of different geometries and working fluids has previously been investigated [48]. The geometry of the loop (pipe diameter, loop shape, inclination angle, heater and cooler orientation, scale and aspect ratio of the loop) is considered as the primary factor that affects the loop performance. Recently, nanofluids have also been used in SPNCLs as a working fluid to increase their performance [62–66], improve the stability [62,66] of the system and reduce the required time to reach a steady state [64].

Investigations on mini SPNCLs (SPNCmL) have been increasing during the last decade. Although there is not any certain criterion for defining an SPNCL as mini, SPNCLs having loop dimensions of tens of centimeters and pipe diameters of a few millimeters are assumed as mini loops. The principle driving mechanisms are the same for the large-scale SPNCLs and SPNCmLs, however, miniaturizing affects system behavior strongly [67]. With the knowledge of enhanced stability by miniaturization of SPNCLs, nanofluids were also used to improve thermo-hydraulic performance and stability of SPNCmLs. Misale et al. [68] studied DIW-based Al_2O_3 nanofluid in an SPNCmL experimentally for the first time. Although using nanofluid improves the thermal performance of SPNCmL slightly for inclined loop orientations, a significant enhancement of thermo-hydraulic performance of the nanofluid-based SPNCmL was not observed compared to DIW. However, results for the mass flow rate inside the loop were in good agreement with the Vijayan's correlation [69], which is one of the important loop characteristics. Turgut and Doganay [70] introduced the effectiveness factor (ε) for the evaluation of the thermal performance of SPNCmLs. ε increases with an increase in nanofluid concentration and decreases with heater power. Karadeniz et al. [71] developed a steady 3D numerical model for predicting the performance and characteristics of the SPNCmLs and validated the model by comparing it with the results of Turgut and Doganay [70]. The deviation from the experimental results was up to 10% for all cases. They concluded that the proposed numerical model is a powerful tool for comparative parametric studies about the performance and characteristics of SPNCmLs.

Doganay and Turgut [72] introduced and evaluated the effectiveness (ε) of Al_2O_3 nanofluid based SPNCmL experimentally at different combinations of inclination angles and heat sink temperatures. ε was calculated higher for lower heat sink temperatures and higher inclination angles. Karadeniz et al. [73] analyzed the experimental results of Doganay and Turgut [72] with their previous model [71]. Koca et al. [74] used a DIW based Ag nanofluid in an SPNCmL and compared the results with a DIW based Al_2O_3 nanofluid. SPNCmL using a lower concentration of Ag nanofluid (0.25 wt.%) had the same thermal stability with DIW as a working fluid. However, the Al_2O_3 nanofluid had an almost constant ε ratio at different heater powers while for higher concentrations of Ag-nanofluid, ε increased significantly with increasing heater power.

Experimental and numerical attempts to represent the performance and characteristics were important for understanding and improving a single SPNCmLs behavior. However, their in-situ characteristics must be well predicted to match them with other components for designing a system properly. SPNCLs can be used for heating and cooling purposes. Therefore, Nu correlations for the hot and cold ends are needed for correctly placing them into an application. Ho et al. [75] used a mini-channel heat sink and heat source to investigate a nanofluid based SPNCmL and proposed

Nu correlations for both heating and cooling ends. They showed that an increase in concentration increases the average Nu number for both ends. In addition, at constant hot wall temperature, cold wall temperature rise causes a reduction of Nu in the heating section unlike the increments in the cooling section. Although an increase in Ra number increases the Re_{ss} number; at constant Ra, Re_{ss} decreases with the addition of nanoparticles. Moreover, they also developed a correlation for Re_{ss} as a function of nanofluid concentration and Gr_m to generalize the characteristics of the system. On the other hand, Mohan et al. [76] used mineral oil based-hexagonal boron nitride nanofluid in SPNCmL. Using nanofluid increased ΔT_{heater} , flow rate and maximum Nu number. They also compared the Re_{ss} predicted by Vijayan's correlation [69] and experiments and they reported the reason behind the deviation in Re_{ss} as the incapability of existing thermophysical property models for oils and nano-oils.

As mentioned above, thermophysical properties of nanofluids are defined either by measurements or theoretical models in the literature. Correct definition of thermophysical properties of nanofluids is crucial for the realistic evaluation of a heat transfer systems' performance. Duangthongsuk and Wongwises investigated both the effect of thermophysical property models [77] and the determination by either MTP or PTP [78] on the calculation of convective heat transfer of a double-tube counter-flow heat exchanger under turbulent flow conditions, experimentally. It is found that different models gave different results, and various models had no significant effect on the heat transfer coefficient and Nu number. Although, MTP had higher values compared to PTP of thermal conductivity and viscosity, the discrepancy between PTP and MTP for the calculation of Nu was found as a few percentages. Recently, Yıldız et al. [79] numerically compared the MTP and PTP in a natural convection cavity under laminar flow conditions and found that PTP utilization underestimated the heat transfer enhancement.

To the best of the authors' knowledge, there are a few studies in the literature on the effect of the determination of thermophysical properties (MTP or PTP) on the overall system performance but there is no study so far for SPNCLs. An SPNCmL is used in this study, which is one of the candidates for the acceleration of nanofluid's market uptake because of its passive nature. As SPNCLs are used to manage a heat transfer need robustly, their in-situ characteristics must be predicted before assembly. This is important for predicting the overall system performance both at design-range and off-design conditions. Within this scope, the main question of this study is how the definition of nanofluids' viscosity and thermal conductivity affect this natural convection-driven heat transfer system's performance prediction. Performance and characteristics of an SPNCmL working with DIW based- Al_2O_3 nanofluid (1, 2 and 3 vol.%) are evaluated for different pipe diameters (3–6 mm). Furthermore, the effects of nanofluids' thermophysical property prediction method on SPNCmL characteristics and performance has been investigated for the first time.

2. Materials and Methods

2.1. Numerical Model

Computer simulations of this study have been done by using a pre-validated numerical methodology [73]. Nanofluid is assumed as a single-phase fluid in the steady 3D numerical model, and validation of the model with experimental results of Doganay and Turgut [72] is also re-reported briefly in Section 3.1. The schematic of geometry, as well as, the parameter table including the dimensions and boundary conditions are given in Figure 1. In the heater part, constant heat flux (corresponding to 10, 30 and 50 W of heat rates for the heater surface area) was applied as the heater power input, whereas in the cooler part, a constant temperature was defined as 20 °C, which is the cooling fluid temperature.

A commercial software (ANSYS CFX) was used for building the geometry and solving the numerical model (a steady laminar full buoyancy model with temperature-dependent thermophysical properties). The general form of the governing equations for steady-state 3-D incompressible flow with negligible viscous dissipation can be expressed as [80]:

Mass conservation equation:

$$\nabla \cdot (\rho \vec{U}) = 0 \quad (1)$$

Momentum equation:

$$\nabla \cdot (\rho \vec{U} \otimes \vec{U}) = -\nabla P + \nabla \cdot \tau + S_{M,buoyancy} \quad (2)$$

Energy equation:

$$\nabla \cdot (\rho \vec{U} h) = \nabla \cdot (k \nabla T) + \vec{U} \cdot \nabla P + S_E \quad (3)$$

The thermal diffusion in the streamwise/axial direction is also neglected in the calculations. In the governing equations, h is enthalpy (m^2/s^2) and \vec{U} is velocity vector (m/s). S denotes the source of momentum ($\text{kg m}^2/\text{s}^2$) and energy (kg m/s^3). ρ and k are the density (kg/m^3) and thermal conductivity (W/m K) of the fluid, respectively.

τ is stress tensor and given as:

$$\tau = \mu \left(\nabla \vec{U} + (\nabla \vec{U})^T - \frac{2}{3} \delta \nabla \cdot \vec{U} \right) \quad (4)$$

where μ is viscosity (kg/m s) and δ is the Kronecker delta.

The full buoyant method is applied in the numerical method as:

$$S_{M,buoyancy} = (\rho - \rho_{ref})g \quad (5)$$

Here, ρ_{ref} is the reference density of the working fluid, which is calculated at the average fluid temperature in the system and given in Appendix A for all working fluids and investigated cases.

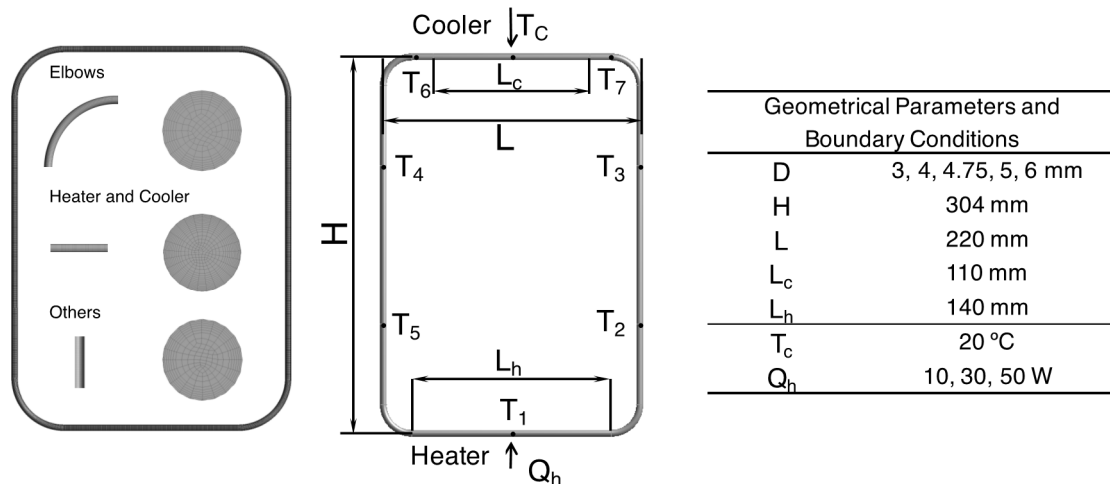


Figure 1. Schematic view of the 3D numerical model geometry, boundary conditions and dimensions.

Since the stability of the SPNCL was improved by miniaturization, the steady numerical model can be used to reduce the computational power (see Section 3.1 for the method validation results). Mesh dependency of the solution was investigated for three different meshes (745,456, 565,681 and 348,087 elements, respectively), all including boundary layer elements to correctly resolve thermal and hydrodynamic boundary layers, in the previous study [73] by comparing temperature difference between hot leg and cold leg (ΔT_{heater}) and maximum temperature (T_{max}), which are the main parameters for comparing experimental and numerical results. The difference is negligible, therefore the coarse mesh number (346,876) was used in the analysis to reduce computational power. The details of the mesh at different parts of the model are presented in Figure 1. Heater and cooler sections of the system have finer boundary layer elements and finer meshes with 0.6 mm of grid size compared to the rest of the system (0.9 mm and 0.8 mm of grid size for elbows and other pipes, respectively) to model precisely. A high-resolution scheme is used to solve advection terms. Convergence criteria were set to 10^{-7} for all of the governing equations in all of the analyses.

2.2. Thermophysical Properties

One of the goals of this study is to understand how the determination of nanofluids' thermophysical properties affects the performance of a representative natural convection heat transfer system. The emphasis is given to the effect of measured and predicted nanofluid thermophysical properties. However, both methods agreed well on some properties (specific heat, density and thermal expansivity). Therefore, only predicted data is used as the input to the numerical simulations for these properties. There is still a discussion on the order-of-magnitude change of the viscosity, and thermal conductivity data, which would lead researchers to misleading results for the prediction of overall system performance. Therefore, both measured and predicted data is used as the input to the numerical simulations for these properties to investigate their effect on overall system performance.

Temperature dependence of thermophysical properties for modeling SPNCmLs is also crucial [73]. Tabular values were used to define the properties for DIW [81] as a function of temperature. However, the existing models to predict nanofluid data do not include temperature effects. Therefore, the temperature dependency of the thermophysical properties was derived by assuming the DIW's temperature dependency as the dominant parameter and using the corresponding equation repetitively for calculating the values at different temperatures. Thermophysical properties of Al_2O_3 nanoparticles are presented in Table 2 [82].

Table 2. Thermophysical properties of Al_2O_3 nanoparticles [82].

	Density ρ_p (kg/m^3)	Specific Heat c_p ($\text{J kg}^{-1} \text{K}^{-1}$)	Thermal Expansion β_p (K^{-1})	Thermal Conductivity k_p ($\text{W m}^{-1} \text{K}^{-1}$)
Al_2O_3	3970	765	0.85	25

The effective specific heat (C_{pe}) values were calculated by Equation (6) [83]. Specific heat does not change with respect to the operational temperature range as seen in Figure 2. Therefore, it is taken as constant for each nanofluid and DIW for the simulations. For Al_2O_3 -DIW nanofluids at different volumetric concentrations (φ), models in the literature were used to determine the effective density (ρ_e) [84] and effective thermal expansion (β_e) [85] as expressed by Equations (7) and (8), respectively (Figure 2). Specific heat does not change within the operational temperature range as seen in Figure 2. Therefore, it is taken as constant for each nanofluid and DIW for the simulations.

$$C_{pe}(\varphi, C_{pp}, \rho_p, \rho_f, C_{pf}, T) = \frac{\varphi(C_{pp}\rho_p) + (1 - \varphi)(\rho_f(T)C_{pf}(T))}{\varphi\rho_p + (1 - \varphi)\rho_f} \quad (6)$$

$$\rho_e(\varphi, \rho_f, T) = (1 - \varphi)\rho_f + \varphi\rho_p, \quad (7)$$

$$\beta_e(\varphi, \beta_p, \rho_p, \rho_f, \beta_f, T) = \frac{\varphi(\beta_p\rho_p) + (1 - \varphi)((\rho_f(T)\beta_f(T))}{\rho_e} \quad (8)$$

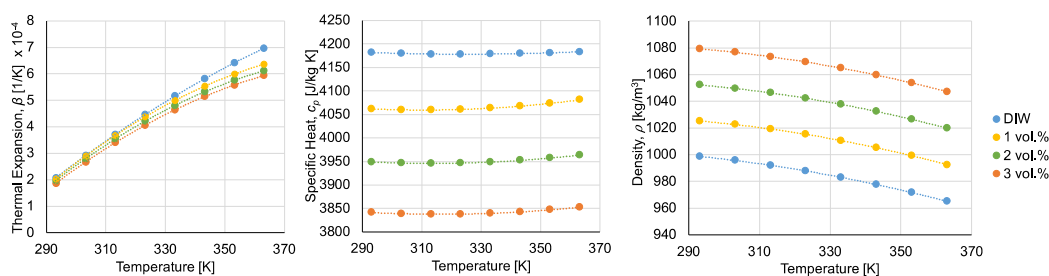


Figure 2. Temperature-dependent thermal expansion, specific heat and density values for working fluids. Both data points and polynomial fits are given in the figure.

The discussion on the viscosity and thermal conductivity of nanofluids is the main focus of this study. Well-known models such as the Maxwell Equation (9) [17] and Einstein Equation (10) [18] correlations have been used for predicting thermal conductivity and viscosity, respectively. These models have been preferred for many nanofluid based system simulations previously.

$$k_{nf}(\varphi, k_p, k_f, T) = \frac{k_p + 2k_f(T) + 2\varphi(k_f(T) - k_p)}{k_p + 2k_f(T) - \varphi(k_f(T) - k_p)} k_f(T), \quad (9)$$

$$\mu_{nf}(\varphi, \mu_f, T) = (1 + 2.5\varphi)\mu_f(T) \quad (10)$$

The measured values reported in [16] were used to prepare the thermal conductivity and viscosity data of MTP. A 3- ω setup and a Brookfield rheometer were used for the measurements of thermal conductivity and viscosity, respectively. Measured and predicted thermal conductivity and viscosity values for working fluids are given in Figure 3. Predicted thermal conductivity data by Maxwell model is slightly higher compared to 3- ω system measurements but they are in good agreement by means of tendency. However, the results of the Einstein viscosity model of nanofluids gives almost concentration independent results compared to measured data. Nevertheless, an increase in temperature closes the gap between measured and predicted viscosity data.

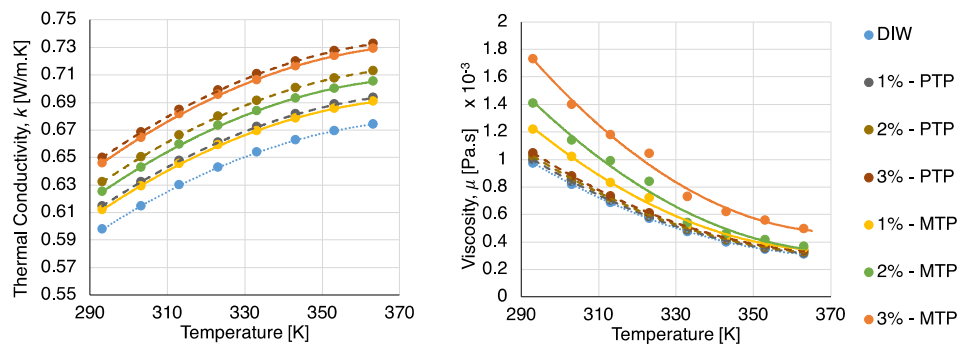


Figure 3. Measured and predicted temperature-dependent thermal conductivity and viscosity values for working fluids. Both data points and polynomial fits (dashed lines for PTP, solid lines for MTP) are given in the figure.

Second-order polynomial functions were fitted to all temperature-dependent thermophysical data in order to define them in the numerical model except for the Einstein correlation for which a fourth-order polynomial was used to increase the accuracy. Thermophysical properties for all working fluids are presented in Figures 2 and 3 and corresponding polynomials are given in Appendix B.

2.3. Performance Indicators

The density gradient due to the temperature difference between heater and cooler sections is the driving mechanism of SPNCLs. Therefore, T_{\max} and ΔT_{heater} can be considered as the main characteristics of SPNCL that are used to compare different operational cases. However, it is possible to observe more information and accurate results on the performance of SPNCLs by calculating mass flow rate and non-dimensional indicators such as ε , Nu , Re_{ss} , Gr_m and Ra . These parameters are defined below. Researchers tend to characterize their systems by using some of these performance indicators but there is not an agreement on which represents the performance more accurately.

Steady-state mass flow rate is a crucial parameter for evaluation of the SPNCLs' performance. Due to the difficulties in the measurement of mass flow rate compared to temperature in real life applications, a theoretical approach that is proposed by Vijayan [69] is mostly used (Equation (11)). This correlation is valid for the natural circulation loops having a uniform diameter (ranging between

4–40 mm), under steady-state conditions with an incompressible Boussinesq fluid, and where the local pressure losses can be neglected. The corresponding mass flow rate in the loop is calculated by [69]:

$$\dot{m} = \left[\frac{2gD^b \rho^2 \beta A^{2-b} Q_h H}{\Delta T p c_p \mu^b N_G} \right]^{1/(3-b)} \quad (11)$$

Here, ΔT is the average temperature difference and N_G is effective loss coefficient and can be calculated as [69]:

$$N_G = \frac{L_{total} \xi}{D f'} \quad (12)$$

where ξ is local friction loss and it is obtained from [82].

During the calculation of the mass flow rate, Re_{ss} can be written as [81]:

$$Re_{ss} = \frac{\dot{m} D}{\mu A}, \quad (13)$$

For the evaluation of a natural convection intensity of the working fluid, the modified Grashoff number (Gr_m) must be determined. Gr_m is the ratio of gravitational forces to shear stresses. For an SPNCL with a stable flow, Gr_m can be determined by [68]:

$$Gr_m = \frac{D^3 \rho^2 Q_h H}{A \mu^3 c_p} \beta g \quad (14)$$

Although Gr_m is used to understand flow characteristics in natural convection, the working fluid that is forced to move while passing along the heating section carries momentum through the loop. Therefore, the system also exhibits forced convection characteristics. For laminar and turbulent flow, Re_{ss} and Gr_m can be correlated by this theoretical approach on mass flow rate [69].

$$Re_{ss} = B \left(\frac{Gr_m}{N_G} \right)^C, \quad (15)$$

where B and C depend on the loop geometrical parameters and working fluid's thermophysical properties. Vijayan defined $B = 0.1768$ and $C = 0.5$ for fully developed laminar flow [69].

ε is defined originally for the heat exchangers, which is a ratio of the actual heat transfer to maximum possible heat transfer. It is also used to understand SPNCL heat transfer performance. ε is defined as:

$$\varepsilon = \frac{T_2 - T_5}{T_2 - T_c}, \quad (16)$$

Moreover, Nu_m is also used for the evaluation of the heat transfer performance of the SPNCLs and is calculated by [86]:

$$Nu_m = \frac{UD}{k}, \quad (17)$$

The overall heat transfer coefficient (U) in Equation (17) was evaluated on the basis of the logarithmic mean temperature difference and it refers to the internal area of the cooler [68]. Overall heat transfer coefficient at the cooler was calculated by using the equations below:

$$U = \frac{Q_h}{\pi D L_c T_{LMTD}}, \quad (18)$$

$$T_{LMTD} = \frac{T_1 - T_2}{\ln(T_1/T_2)}, \quad (19)$$

$$T_1 = T_6 - T_c, \quad (20)$$

$$T_2 = T_7 - T_c, \quad (21)$$

Nu_m can be calculated in the same manner. Ra number is also considered as a non-dimensional performance indicator due to being useful for investigation of the buoyancy-driven heat transfer and it is introduced as [87]:

$$Ra = Gr_m Pr, \quad (22)$$

where Pr is Prandtl number and defined as [87]:

$$Pr = \frac{\mu c_p}{k}, \quad (23)$$

3. Results and Discussion

In this section, firstly validation of the numerical model using experimental results of Doganay and Turgut [72] is reported briefly. Moreover, the thermo-hydraulic performance of SPNCmL for PTP and MTP cases, and for different pipe diameters are discussed in terms of performance parameters to reveal the sensitivity of the system to thermophysical property inputs. As SPNCmLs are passive components that are used to manage a heat transfer process robustly, their in-situ characteristics must be predicted before assembly. This is important for predicting the overall system performance both at design-range and off-design conditions. Therefore, the SPNCmL performance is generalized by introducing Nu correlations for both thermophysical property inputs and the applicability and accuracy of the Nu correlations are discussed afterward.

A legend system that is valid for all the results given in the following sections is introduced as the high number of parameters makes it difficult to conduct the results. Table 3 compiles colors for nanofluids, and pipe diameters and heater powers are presented in Table 4. Moreover, filled symbols are used for 50 W, patterned symbols for 30 W and empty symbols for 10 W. Symbol “X” denotes numerical results of 4.75 mm pipe diameter for the validation study.

Table 3. Colors for working fluids.

















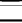
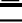
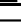
Color	Working Fluid
	DIW
	1% Alumina nanofluid (MTP)
	2% Alumina nanofluid (MTP)
	3% Alumina nanofluid (MTP)
	1% Alumina nanofluid (PTP)
	2% Alumina nanofluid (PTP)
	3% Alumina nanofluid (PTP)

Table 4. Symbols for pipe diameters and heater powers.

Pipe Diameter	Heater Power		
	10 W	30 W	50 W
3 mm			
4 mm			
5 mm			
6 mm			

3.1. Validation

Results of the 3D numerical model for PTP and MTP cases are compared with the experimental results of a well-proven setup [70,72,74] (pipe diameter is 4.75 mm) by means of T_{max} , ΔT_{heater} and ε . Considering MTP results, Figure 4 shows that results obtained from the numerical model have a good agreement with the experimental data. ε , T_{max} and ΔT_{heater} , varied between $\pm 10\%$, $\pm 20\%$ and $\pm 20\%$ error bands, respectively. As shown in Figure 4, ε has the same tendency with the experimental results and increases with the increase in concentration and decreases with the increasing heater power for

both PTP and MTP. Numerical ϵ results are getting closer to experimental results at lower powers. Heater power doesn't affect the accuracy of the T_{\max} results, as it is always over-predicted by the simulation. However, ΔT_{heater} is better predicted as the heater power increases opposite to ϵ results.

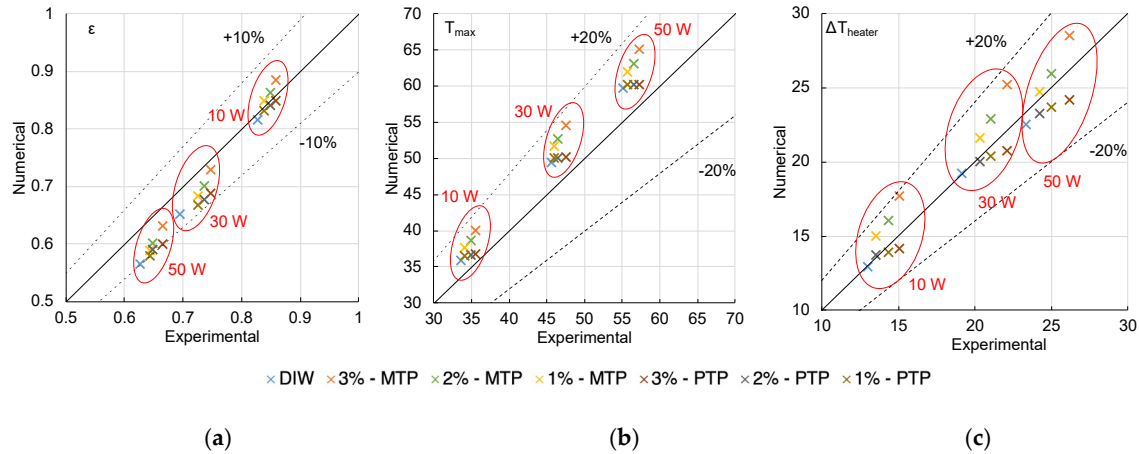


Figure 4. Comparison between the numerical model's results with experimental values of [70,72] in terms of a performance indicator and system characteristics: (a) effectiveness (ϵ), (b) T_{\max} and (c) ΔT_{heater} .

Increase in concentration results in a significant increase of ΔT_{heater} for both MTP and PTP, MTP having a higher slope. As concentration increases, T_{\max} increases significantly for MTP but for PTP a minor change is observed. An increase in viscosity means a higher resistance to flow, which results in lower mass flow rates. The slower motion of the fluid causes higher heat dissipation to the inner layers of the fluid which results in higher average temperatures in cross-sections. Moreover, for all heater powers, DIW results are in good agreement with the experimental results of T_{\max} and ΔT_{heater} . But for ϵ , nanofluids are well-predicted compared to DIW at lower heater powers. To conclude, compared to MTP, PTP results fit well with the experimental study in terms of loop temperatures, which are mainly used to characterize the system. However, for ϵ , which is a performance indicator, as heater power increases PTP results diverge more from the experimental data compared to that of MTP. Therefore, it is not easy to choose one or the other by means of a validation study.

3.2. MTP and PTP Comparison for Different Pipe Diameters

A set of pipe diameters (3, 4, 5 and 6 mm) was selected to extend the operating range with the aim of the generalization of the results for the SPNCmL performance and improve the discussion on MTP and PTP cases. Loop temperatures (T_{\max} and ΔT_{heater}) for different pipe diameters are reported in Figure 5 together with MTP and PTP comparison with $\pm 15\%$ deviation bands. For MTP, T_{\max} and ΔT_{heater} increase with the increase in heater power and concentration of nanofluid as shown in Figure 5. Power-dependent groups (i.e., empty, striped and filled) of data are observed for both T_{\max} and ΔT_{heater} . Moreover, the addition of nanoparticles into DIW increases the T_{\max} and ΔT_{heater} , which means an increase in SPNCmL implementation potential in thermal systems due to higher temperatures. The same behavior has been reported in the literature [70,71,73,76]. However, Bejjam and Kumar [88] said that nanofluids decrease the temperature difference between hot and cold legs. In another study [89], it was reported that for up to 5% vol. concentration temperature difference at the heater increases with the increase in heater power but at 6% vol. it decreases.

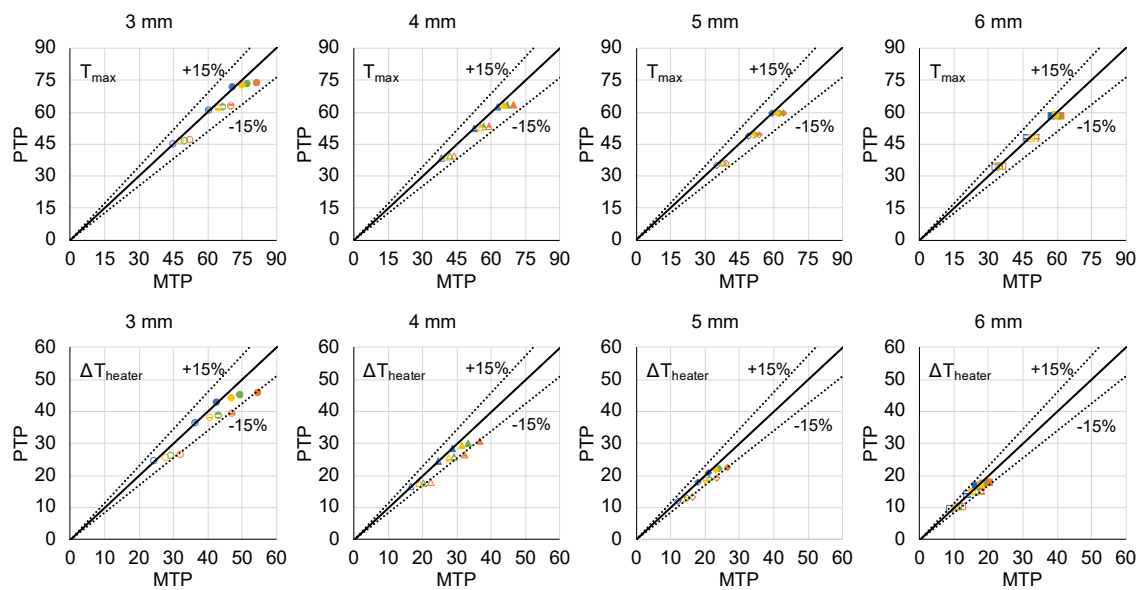


Figure 5. T_{\max} and ΔT_{heater} values at different pipe diameters for MTP and PTP, and MTP and PTP comparison with $\pm 15\%$ deviation bands.

By using PTP, Figure 5 shows that the concentration effect on T_{\max} and ΔT_{heater} is small compared to MTP and concentration-dependent difference decreases with the increase in pipe diameter. This effect can be seen slightly in Figure 4 but is more apparent in Figure 5 due to the increased operational range by changing the pipe diameter. The main difference between MTP and PTP is at viscosity values (Figure 3), namely; viscosity is almost unaffected by the particle content when Einstein correlation was used. Therefore, it is thought that this difference is directly related to the viscosity data for the PTP. As pipe diameter increases, the total mass in the SPNCmL increases and results in a higher heat capacity of the working fluid. For constant heat flux boundary conditions, higher heat capacity decreases for both T_{\max} and ΔT_{heater} as shown in Figure 5. A smaller ΔT_{heater} closes the viscosity range during operation (Figure 3) and thus, the difference between the T_{\max} data of PTP and MTP decreases.

ε totally depends on the temperatures of the SPNCmL (Equation (16)). Therefore, similar trends with temperatures are observed for ε , too. As presented in Figure 6, ε decreases with the increase in heater power for different loop diameters for both cases. For higher heater powers, ΔT_{heater} and T_{\max} have higher values, and as a consequence ε increases. The previous studies [70–73] in the literature have reported that ε increases with an increase in nanofluid concentration. In this study, it is also found that increments in concentration for all diameters enhance effectiveness as a result of higher temperatures. Contrary to the effect of concentration, a decrease in pipe diameter results in an enhancement in ε . Sahu and Sarkar [90] reported that ε decreases with the increased pipe diameter within the range of 25–30 mm, which is much higher than the pipe diameter range considered in this study. Due to the insignificant concentration dependency of viscosity to temperatures for the PTP case (Figure 3), change in ε with concentration is smaller than MTP. However, as shown in Figure 6, decreasing the pipe diameter to below 3 mm would not enhance ε at lower powers for both MTP and PTP based systems because the limit for ε is unity. To conclude, SPNCmLs with smaller pipe diameters at higher heater power have an improved potential to be used in thermal applications.

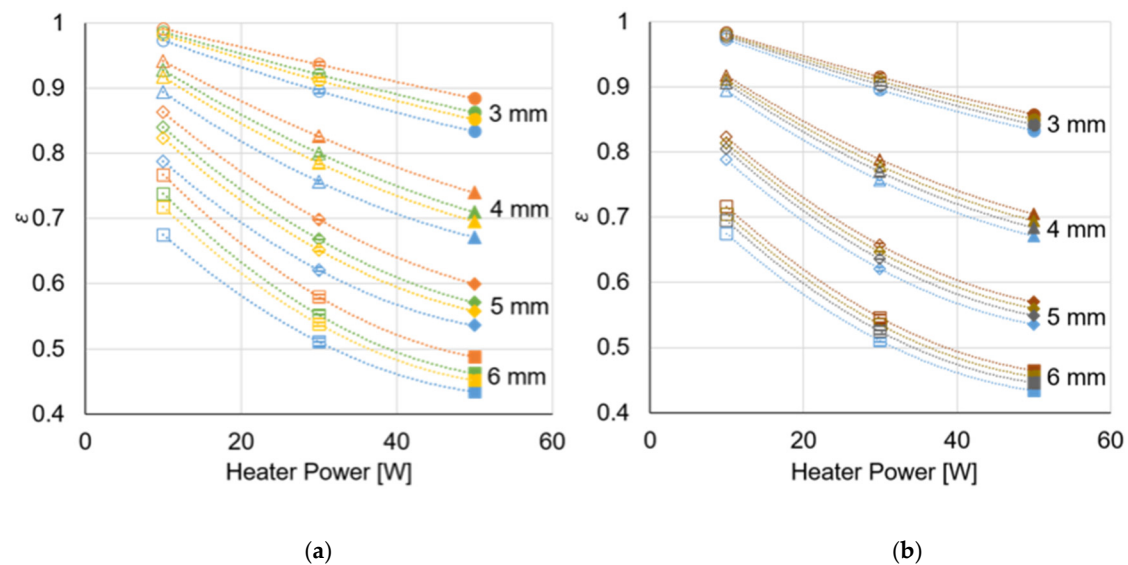


Figure 6. Effectiveness at different pipe diameters for (a) MTP and (b) PTP.

As seen from loop temperature and effectiveness results, the definition of the thermophysical properties with existing correlations or experiments affects the performance evaluation of the SPNCmL. ε is used to predict overall performance of SPNCmL and it is related to temperature differences. In this case, using MTP is thought to be more accurate than PTP.

3.3. Generalization of Results

Characterization parameters and effectiveness are not sufficient to understand the performance of the SPNCmLs and to conclude on the PTP and MTP selection. Therefore, non-dimensional parameters are used to generalize the discussion on SPNCmL performance for both thermophysical property inputs. In this study, widely used dimensionless parameters have been used to evaluate pipe diameter, working fluid, and MTP and PTP cases' effects on thermo-hydraulic performance. Although the flow inside SPNCs is driven by density difference arising from the temperature change, a representative Reynold's number for the steady flow (Re_{ss}) can be calculated as given previously in Equation (13). Mass flow rate values obtained from the numerical study were used to calculate Re_{ss} in this study. A correlation developed by Vijayan [69] that is valid for fully developed laminar flows for SPNCs (not mini) and for a wide pipe diameter range (4–40 mm) is used for comparison. Effective loss coefficient (N_G) and modified Grashoff number (Gr_m) were calculated by Equations (12) and (14) by handling the data obtained from the simulations for this purpose. The results were compared with Vijayan's correlation (Equation (15)) to check the validity of the correlation for different pipe diameters of SPNCmL (Figure 7). As seen in Figure 7, the discrepancy between the simulation results and Vijayan's correlation is up to 50% for the MTP case and up to 45% for the PTP case.

As seen in Figure 7a,b the data is grouped by the pipe diameters (i.e., circles, triangles, diamonds and squares) firstly and then heater power groups are distinguished (i.e., empty, striped and filled). Re_{ss} increases (because of the mass flow rate increase) with the increase in heater power for both cases and decreases as the concentration increases for MTP cases. However, concentration-dependent distribution of PTP data points is less compared to MTP but PTP data in Figure 7b shows that the change of Re_{ss} with concentration is insignificant. The main reason behind this behavior could be the minor change of viscosity with concentration for the PTP case. Bejjam and Kumar [89] (studied numerically and used the mixture rule for both thermal conductivity and viscosity data) have found that Re_{ss} increases with the heater power but an increase in concentration also increases the Re_{ss} contrary to MTP and PTP results obtained in this study. Nayak et al. [62,66] (studied experimentally and used the Hamilton–Crosser model for thermal conductivity and Brinkman for viscosity data), Thomas et

al. [91] and Thomas and Sobhan [63] (studied experimentally and used the THW method such as KD2 Pro data for thermal conductivity and unknown for viscosity) have reported that Re_{ss} increased with the concentration. Moreover, Ho et al. [75] (studied numerically and used KD2 Pro data for thermal conductivity and Brookfield rheometer data for viscosity) reported that concentration of the nanofluid has a higher impact on Re_{ss} .

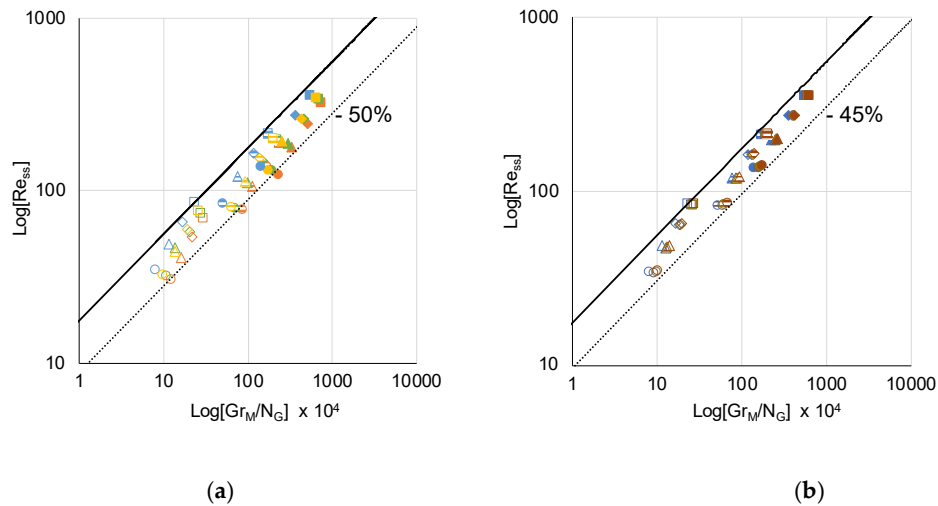


Figure 7. Comparison of the results with the Vijayan's correlation (Equation (15)) for (a) MTP and (b) PTP cases.

Besides concentration, Re_{ss} increases with pipe diameter for all heater powers in this study. Since the system has a higher total mass for higher pipe diameters, mass flow rate and thus, Re_{ss} increases. For higher pipe diameters, the reduction of Re_{ss} compared to DIW has increased for MTP. As the heater power increases, Gr_m increases. In addition to heater power, Gr_m also increases with the increase in loop diameter as Re_{ss} but it also increases with the concentration in contrary to Re_{ss} for both MTP and PTP. For the MTP case, Gr_m range is 1.93×10^7 – 9.45×10^8 and Re_{ss} range is 30–355; and for the PTP case, Gr_m varies in the range of 1.93×10^7 – 7.97×10^8 and Re_{ss} range is 34–358. Although, concentration effects are smaller on Gr_m as well as Re_{ss} , the minor dependency of viscosity on concentration for the PTP case (Figure 3) results in a smaller change of Gr_m compared to MTP.

Figure 7 shows a significant difference between the Vijayan's correlation (Equation (10)) and the numerical results of this study. The deviation is more for the MTP case. Vijayan's correlation (Equation (10)) is valid for fully developed laminar flows for SPNCLs (not mini) and for a wide pipe diameter range (4–40 mm). It is clear that pipe dimensions and heater power values are at a smaller range for this study and they affect the flow characteristics together with the concentration, increasing the deviation from the Vijayan's correlation (Equation (10)).

The addition of nanoparticles or an increase in concentration decreases the mass flow rate and Re_{ss} . Therefore, results shifted below the correlation as shown in Figure 7a,b. In order to correlate this shift for DIW and different nanofluid concentrations, a concentration-dependent Re_{ss} model for nanofluid based SPNCmLs has been developed by using the numerical results. The correlation which is valid for the working fluids within a concentration range of $\phi = 0$ –3% and $10^4 \leq \frac{Gr_m}{N_G} \leq 10^7$ is given in Equation (24) and the plot is given in Figure 8. This correlation is more accurate (data scattering is reduced to 20% bandwidth, which was previously up to 50%) for both the MTP and PTP cases compared to the Vijayan's correlation.

$$Re_{ss} = (0.06) \left(\frac{Gr_m}{N_G} \right)^{0.53} Pr^{0.3}, \quad (24)$$

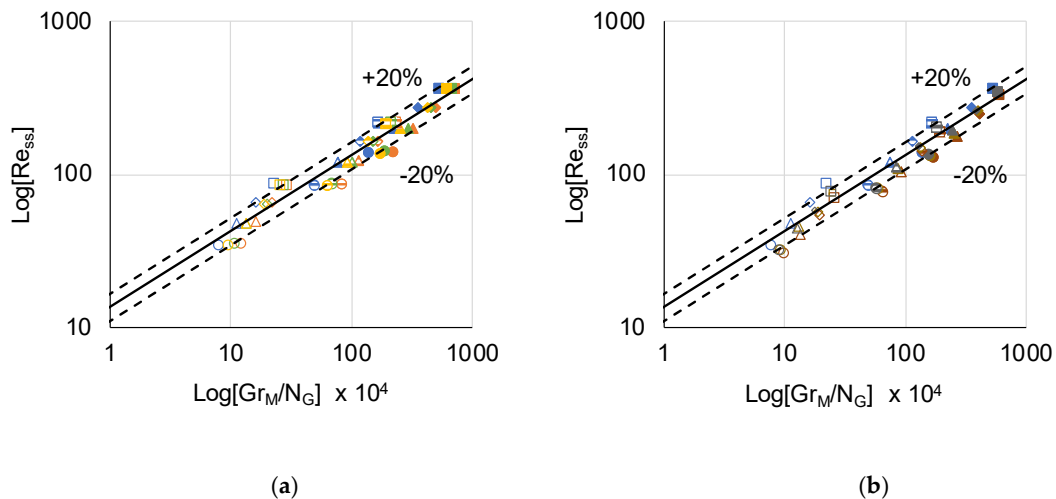


Figure 8. Concentration dependent Re_{ss} model for nanofluid based SPNCmLs for (a) MTP and (b) PTP.

As NCLs are passive components that are used to manage a heat transfer need robustly, their in-situ characteristics must be predicted before assembly. This is important for predicting the overall system performance both at design-range and off-design conditions. A wide operational range description of the characteristics of NCLs can be predicted by the dimensionless heat transfer coefficient, the modified Nusselt number (Nu_m). SPNCmLs (also all NCLs) can be used for heating or cooling purposes. Therefore, a Nu_m can be defined either for the heater or for the cooler section. Most of the previous studies on SPNCLs applied constant temperature boundary condition in the heater section and developed Nu_m correlations as a function of Ra [92] and Re_{ss} [93]. Different from the related literature, in this study, a nanofluid based SPNCmL is aimed to be used for thermal applications with the heating purpose.

Figure 9 presents the relationship of Nu_m for the cooler section with Ra for constant temperature boundary condition. It is obvious that higher heater powers cause a higher Ra and Nu_m as expected for both PTP and MTP. Nu_m decreases as the nanoparticle concentration increases for constant Ra for both cases. Reduction in Nu_m with concentration could be due to neglecting the Brownian motion and thermophoresis effects in the numerical simulations [94]. Moreover, as the pipe diameter increases Nu_m decreases and Ra increases for all working fluids (for both MTP and PTP cases) and heater powers.

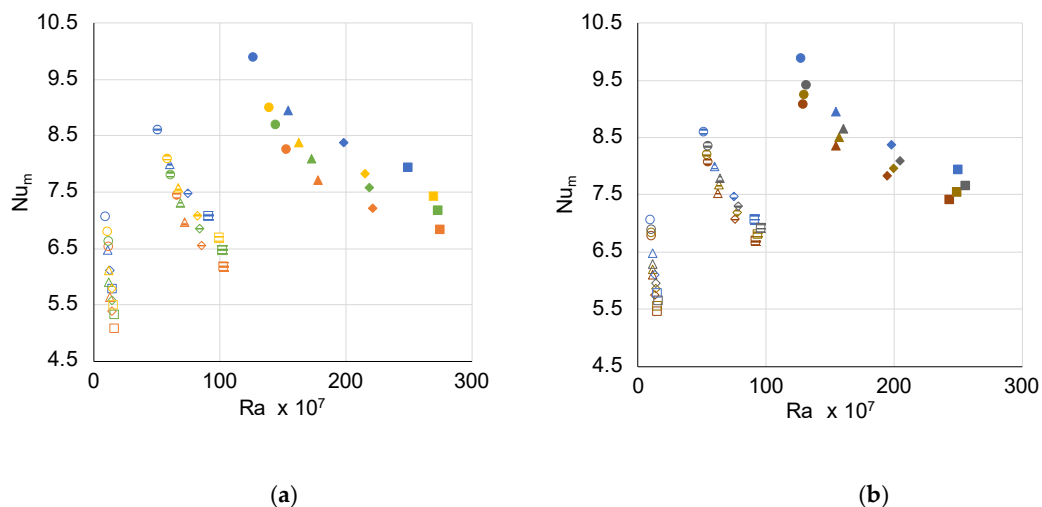


Figure 9. Change of Nu_m with Ra for (a) MTP and (b) PTP.

Changing working fluid and heater powers result in changes of thermophysical properties and thus Re_{ss} , Gr_m and Pr . Figure 9 shows that evaluating Nu_m with respect to Ra results in groups with regard to pipe diameter and heater power. Therefore, numerical results are used to develop a correlation for Nu_m at the cooler section considering a shape factor ($\frac{L_c}{D}$) for generalization (Equation (25)), consistent with the previous literature [92].

As shown in Figure 10, $Nu_{m,c} = f(\frac{L_c}{D}, Ra)$ is applicable for SPNCmLs working with different fluids at various pipe diameters. Results show that the correlation given in Equation (25), has a discrepancy of $\pm 7\%$ for both MTP and PTP cases. Considering the deviation of the numerical study from the experimental results (Figure 4), the overall error of the proposed correlations is not more than 20%, which is acceptable for the design purposes of a system including an SPNCmL.

$$Nu_{m,c} = 0.00025 \left(\frac{L_c}{D} Ra^{0.3} \right) + 4.5, \quad (25)$$

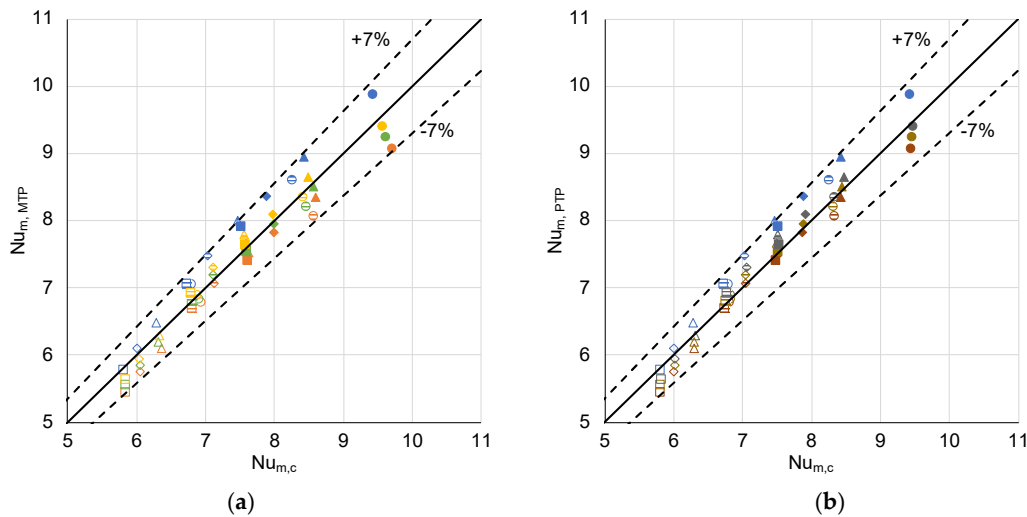


Figure 10. Validation of $Nu_{m,c}$ correlation for (a) MTP and (b) PTP.

4. Conclusions

Correct prediction of the thermophysical properties has great importance for investigating the nanofluid's effect on the performance of the heat transfer systems. Due to restrictions arising from the increased viscosity of nanofluids, passive heat transfer systems have great potential in nanofluid's market uptake. SPNCmLs, as passive systems, are widely used in the solar thermal applications and nuclear cooling systems in which nanofluids' potential is also comprehensively studied. In this study, the influence of thermophysical property definition on the performance of nanofluid based SPNCmLs has been studied numerically. Results of measured thermophysical properties (MTP) and predicted thermophysical properties (PTP) have been compared by using DIW and DIW based Al_2O_3 nanofluid (1, 2 and 3 vol.%). Numerical study was conducted for different pipe diameters to broaden the operating range. Several major conclusions are presented as follows:

- The thermal conductivity of PTP results are in good agreement with the MTP data. However, for viscosity, MTP results are higher compared to PTP and the gap between MTP and PTP results is close with the increase in temperature;
- Validation of 3D steady state model is studied by using experimental results in terms of performance parameters for both PTP and MTP. ε , T_{max} and ΔT_{heater} exhibit the same trend as experimental data within $\pm 10\%$, $\pm 20\%$ and $\pm 20\%$ error bands, respectively. Therefore, the numerical model is sufficient for a parametric study. Compared to MTP results, PTP data fits well with the experimental study in terms of T_{max} and ΔT_{heater} ;

- Nanofluids have higher ε , T_{\max} and ΔT_{heater} values compared to DIW for the whole power range. However, PTP results have tiny changes compared to MTP. ε decreases with the increase of heater power whereas T_{\max} and ΔT_{heater} increase. Higher pipe diameters result in a reduction in ε , T_{\max} and ΔT_{heater} for all working fluids and input powers;
- Dimensionless numbers are expected to dissipate the dimensional effects on the performance characteristics. Therefore, $Re_{ss}-\frac{Gr_m}{N_G}$ and $Ra-Nu_m$ charts are prepared for both MTP and PTP;
- Nu at the cooler section decreases with the concentration in SPNCLs;
- Although nanofluids have smaller Nu_m at the cooler section compared to DIW, ε of the overall system is higher for nanofluids. The reason behind the reduction of Nu_m could be the Brownian motion and thermophoresis effects of particles;
- The concentration-dependent mass flow rate model was introduced for nanofluid based SPNCmLs, which is valid for working fluids with concentrations between $\varphi = 0\text{--}3\%$ and $10^4 \leq \frac{Gr_m}{N_G} \leq 10^7$, and more accurate than Vijayan's correlation;
- Nu_m correlation for the cooler section is defined as $Nu_m = f(\frac{L_c}{D}, Ra)$ to generalize the heat transfer performance of SPNCmL;
- The difference between predicted thermal conductivity and viscosity of nanofluids by well-known models and measured data does not affect the heat transfer performance significantly.

To conclude, the effect of the thermal conductivity on SPNCmL characteristics is found to be limited for the investigated cases. However, viscosity affects the SPNCmL characteristics significantly as the viscosity values differ greatly for both the measured and Einstein correlation's data. Thermo-hydraulic performance is also evaluated by calculating the dimensionless heat transfer coefficient. A Nu correlation is introduced for the investigated SPNCmL model, which is useful for implementing the SPNCmL into a solar thermal system. The methodology proposed in this study can be used to derive Nu correlations for different geometries.

Author Contributions: Z.H.K. prepared the numerical model and computer simulations. N.Ç. produced computational results, figures and tables. N.Ç. wrote the draft and Z.H.K. finalized the paper. All authors have read and agreed on the published version of the manuscript.

Funding: This research received no external funding.

Conflicts of Interest: The authors declare no conflict of interest.

Nomenclature

3D	Three dimensional
A	Flow area (m^2)
b	Constant of $f = p/Re^b$
B	Constant at $Re_{ss} = B\left(\frac{Gr_m}{N_G}\right)^C$
C	Constant at $Re_{ss} = B\left(\frac{Gr_m}{N_G}\right)^C$
c_p	Specific heat (J/kg K)
D	Inner pipe diameter (m)
DIW	Distilled water
EG	Ethylene glycol
f	Friction factor
g	Gravitational acceleration (m/s^2)
Gr	Grashof number
H	Height of loop (m)
k	Thermal conductivity of the working fluid (W/mK)
L	Length (m)

L_{total}	Total pipe length (m)
MTP	Measured thermophysical properties
\dot{m}	Mass flow rate (kg/s)
NCL	Natural circulation loop
N_G	Effective loss coefficient
N_t	Total number of pipe segments
Nu	Nusselt number
p	Constant of $f = p/Re^b$
P	Pressure (kg/m s ²)
PTP	Predicted thermophysical properties
Pr	Prandtl number
Q	Heater power (W)
Ra	Rayleigh number
Re_{ss}	Steady state Reynolds number
SPNCLs	Single phase natural circulation loops
SPNCmLs	Single phase natural circulation mini loops
T	Temperature (°C)
ΔT	Fluid temperature difference (°C)
U	Overall heat transfer coefficient (W/m ² K)
\vec{U}	Velocity vector (m/s)

Greek Symbols

ε	Effectiveness
δ	Kronecker delta function
ρ	Density (kg/m ³)
β	Thermal expansivity (1/K)
φ	Volumetric concentration
μ	Viscosity (Pa.s)
ξ	Local heat transfer loss
τ	Stress tensor
\emptyset	Particle diameter

Subscriptions

c	Cooler
e	Effective
E	Energy
f	Fluid
g	General
i	Inlet
LMTD	Logarithmic mean temperature difference
m	Modified
M	Momentum
max	Maximum
nf	Nanofluid
p	Particle
ref	Reference

Appendix A. Reference Density Values of Working Fluids

Buoyancy calculations in the solution require density difference ($\rho - \rho_{ref}$) and using ρ_{ref} results with the exclusion of hydrostatic gradient of the pressure in the momentum equation. ρ_{ref} is calculated at the average fluid temperature for all investigated cases. ρ_{ref} values of the simulations are presented in Table A1.

Table A1. ρ_{ref} values of working fluids at different heater powers.

Working Fluid	ρ_{ref} (kg/m ³)		
	10 W	30 W	50 W
DIW	995.83	992.150	988.554
1 vol. %	1022.579	1019.137	1015.766
2 vol. %	1049.560	1045.890	1042.764
3 vol. %	1076	1073	1069

Appendix B. Polynomials for Thermophysical Properties of Working Fluids

Thermophysical properties of working fluids were applied to the numerical model as temperature-dependent polynomial functions of the data presented in Figures 2 and 3.

Temperature-dependent thermophysical properties of DIW used in the numerical model are presented as follows:

$$k_{DIW} = 0.6065 \left(a_1 + a_2 \left(\frac{T}{T_{ref}} \right) + a_3 \left(\frac{T}{T_{ref}} \right)^2 \right), \quad (A1)$$

Here, $a_1 = -1.48445$, $a_2 = 4.12292$ and $a_3 = -1.63866$ with the unit of (W/(m K)) for all constants and the reference temperature (T_{ref}) is 298.15 K.

$$\mu_{DIW} = b_1 10^{\frac{b_2}{T-b_3}}, \quad (A2)$$

where $b_1 = 2.414 \times 10^{-5}$ (N s/m²), $b_2 = 247.8$ (K) and $b_3 = 140$ (K).

Thermal expansion coefficient of DIW is expressed as:

$$\beta_{DIW} = c_1 T + c_2, \quad (A3)$$

Here, $c_1 = 0.000007$ (K⁻²) and $c_2 = 0.00183$ (K⁻¹).

And finally, the temperature-dependent density equation of DIW is applied as:

$$\rho_{DIW} = d_1 T^2 + d_2 T + d_3, \quad (A4)$$

with constants for $d_1 = -0.002992$ (kg/(K² m³)), $d_2 = 1.4824$ (kg/(K m³)), $d_3 = 821.27$ (kg/m³).

For nanofluids, second order polynomials are developed for both MTP and PTP but a fourth order equation is used to improve the accuracy of Einstein's viscosity model.

$$k_{MTP \& PTP} = a_1 T^2 + a_2 T + a_3, \quad (A5)$$

$$\mu_{PTP} = b_1 T^4 + b_2 T^3 + b_3 T^2 + b_4 T + b_5, \quad (A6)$$

$$\mu_{MTP} = b_3 T^2 + b_4 T + b_5, \quad (A7)$$

$$\beta_{MTP \& PTP} = c_1 T^2 + c_2 T + c_3, \quad (A8)$$

$$\rho_{MTP \& PTP} = d_1 T^2 + d_2 T + d_3, \quad (A9)$$

$$c_{p_{MTP \& PTP}} = e_1 T^2 + e_2 T + e_3, \quad (A10)$$

Table A2. Constants in polynomials of thermophysical properties of nanofluids.

Thermal Conductivity					
	a_1 (W m ⁻¹ K ⁻³)	a_2 (W m ⁻¹ K ⁻²)	a_3 (W m K ⁻¹)		
MTP-1 vol.%	-1.0717×10^{-5}	8.1541×10^{-3}	-8.5753×10^{-1}		
MTP-2 vol.%	-1.0948×10^{-5}	8.3294×10^{-3}	-8.7598×10^{-1}		
MTP-3 vol.%	-1.1314×10^{-5}	8.6084×10^{-3}	-9.0531×10^{-1}		
PTP-1 vol.%	-1.1484×10^{-5}	8.6139×10^{-3}	-9.2368×10^{-1}		
PTP-2 vol.%	-1.1792×10^{-5}	8.8443×10^{-3}	-9.4739×10^{-1}		
PTP-3 vol.%	-1.2105×10^{-5}	9.0788×10^{-3}	-9.7150×10^{-1}		
Viscosity					
	b_1 (N s m ⁻² K ⁻⁴)	b_2 (N s m ⁻² K ⁻³)	b_3 (N s m ⁻² K ⁻²)	b_4 (N s m ⁻² K ⁻¹)	b_5 (N s m ⁻²)
MTP-1 vol.%	-	-	1.4435×10^{-7}	-1.0732×10^{-4}	2.0283×10^{-2}
MTP-2 vol.%	-	-	1.6339×10^{-7}	-1.2249×10^{-4}	2.3285×10^{-2}
MTP-3 vol.%	-	-	1.9613×10^{-7}	-1.4639×10^{-4}	2.7783×10^{-2}
PTP-1 vol.%	3.4020×10^{-11}	-4.6467×10^{-8}	2.3846×10^{-5}	-5.4559×10^{-3}	4.7051×10^{-1}
PTP-2 vol.%	3.4850×10^{-11}	-4.7600×10^{-8}	2.4428×10^{-5}	-5.5890×10^{-3}	4.8198×10^{-1}
PTP-3 vol.%	3.5679×10^{-11}	-4.8733×10^{-8}	2.5010×10^{-5}	-5.7221×10^{-3}	4.9346×10^{-1}
Thermal Expansion					
	c_1 (K ⁻³)	c_2 (K ⁻²)		c_3 (K ⁻¹)	
MTP and PTP-1 vol.%	-4.0280×10^{-8}	3.2627×10^{-5}		-0.0059	
MTP and PTP-2 vol.%	-3.8600×10^{-8}	3.1260×10^{-5}		-0.00565	
MTP and PTP-3 vol.%	-3.7400×10^{-8}	3.0360×10^{-5}		-0.0055	
Density					
	d_1 (kg K ⁻² m ⁻³)	d_2 (kg K ⁻¹ m ⁻³)		d_3 (kg m ⁻³)	
MTP and PTP-1 vol.%	-3.3440×10^{-3}	1.7275		806.17	
MTP and PTP-2 vol.%	-3.3150×10^{-3}	1.7119		835.245	
MTP and PTP-3 vol.%	-3.2760×10^{-3}	1.6915		864.86	
Specific Heat					
	e_1 (J kg ⁻¹ K ⁻³)	e_2 (J kg ⁻¹ K ⁻²)		e_3 (J kg ⁻¹ K ⁻¹)	
MTP and PTP-1 vol.%	0.0079	-4.8904		4819.1	
MTP and PTP-2 vol.%	0.0072	-4.5219		4654.3	
MTP and PTP-3 vol.%	0.0069	-4.3851		4531.4	

References

- Assael, M.J.; Antoniadis, K.D.; Wakeham, W.A.; Zhang, X. Potential applications of nanofluids for heat transfer. *Int. J. Heat Mass Transf.* **2019**, *138*, 597–607. [\[CrossRef\]](#)
- Buschmann, M.; Azizian, R.; Kempe, T.; Julia, J.E.; Martínez-Cuenca, R.; Sundén, B.; Wu, Z.; Seppälä, A.; Ala-Nissila, T. Correct interpretation of nanofluid convective heat transfer. *Int. J. Therm. Sci.* **2018**, *129*, 504–531. [\[CrossRef\]](#)
- Bobbo, S.; Fedele, L. Experimental Methods for the Characterization of Thermophysical Properties of Nanofluids. In *Heat Transfer Enhancement with Nanofluids*; CRC Press: Boca Raton, FL, USA, 2015; pp. 103–130.
- Sundar, L.S.; Sharma, K.; Naik, M.; Singh, M.K. Empirical and theoretical correlations on viscosity of nanofluids: A review. *Renew. Sustain. Energy Rev.* **2013**, *25*, 670–686. [\[CrossRef\]](#)
- Gupta, M.; Singh, V.; Kumar, R.; Said, Z. A review on thermophysical properties of nanofluids and heat transfer applications. *Renew. Sustain. Energy Rev.* **2017**, *74*, 638–670. [\[CrossRef\]](#)
- Koca, H.D.; Doğanay, S.; Turgut, A.; Tavman, I.H.; Saidur, R.; Mahbubul, I.M. Effect of particle size on the viscosity of nanofluids: A review. *Renew. Sustain. Energy Rev.* **2018**, *82*, 1664–1674. [\[CrossRef\]](#)
- Murshed, S.M.S.; Estellé, P. A state of the art review on viscosity of nanofluids. *Renew. Sustain. Energy Rev.* **2017**, *76*, 1134–1152. [\[CrossRef\]](#)
- Tawfik, M.M. Experimental studies of nanofluid thermal conductivity enhancement and applications: A review. *Renew. Sustain. Energy Rev.* **2017**, *75*, 1239–1253. [\[CrossRef\]](#)
- Yang, L.; Xu, J.; Du, K.; Zhang, X. Recent developments on viscosity and thermal conductivity of nanofluids. *Powder Technol.* **2017**, *317*, 348–369. [\[CrossRef\]](#)

10. Doğanay, S.; Alsangur, R.; Turgut, A. Effect of external magnetic field on thermal conductivity and viscosity of magnetic nanofluids: A review. *Mater. Res. Express* **2019**, *6*, 112003. [\[CrossRef\]](#)
11. Antoniadis, K.D.; Tertsinidou, G.J.; Assael, M.J.; Wakeham, W.A. Necessary Conditions for Accurate, Transient Hot-Wire Measurements of the Apparent Thermal Conductivity of Nanofluids are Seldom Satisfied. *Int. J. Thermophys.* **2016**, *37*, 78. [\[CrossRef\]](#)
12. De Castro, C.A.N.; Lourenço, M.J.V. Towards the Correct Measurement of Thermal Conductivity of Ionic Melts and Nanofluids. *Energies* **2019**, *13*, 99. [\[CrossRef\]](#)
13. Zendejboudi, A.; Saidur, R. A reliable model to estimate the effective thermal conductivity of nanofluids. *Heat Mass Transf.* **2018**, *55*, 397–411. [\[CrossRef\]](#)
14. Alawi, O.A.; Azwadi, N.; Xian, H.W.; Kean, T.H.; Kazi, S. Thermal conductivity and viscosity models of metallic oxides nanofluids. *Int. J. Heat Mass Transf.* **2018**, *116*, 1314–1325. [\[CrossRef\]](#)
15. Murshed, S.M.S.; Leong, K.; Yang, C. Investigations of thermal conductivity and viscosity of nanofluids. *Int. J. Therm. Sci.* **2008**, *47*, 560–568. [\[CrossRef\]](#)
16. Turgut, A.; Saglanmak, S.; Doganay, S. Experimental investigation on thermal conductivity and viscosity of nanofluids: Particle size effect. *J. Fac. Eng. Archit. Gazi Univ.* **2016**, *31*, 95–103.
17. Maxwell, J.C. *A Treatise on Electricity and Magnetism*; Clarendon Press: Oxford, UK, 1881; Volume 1.
18. Einstein, A. Eine neue Bestimmung der Moleküldimensionen. *Ann. der Phys.* **1906**, *324*, 289–306. [\[CrossRef\]](#)
19. Nguyen, C.; Desgranges, F.; Galanis, N.; Roy, G.; Mare, T.; Boucher, S.; Mintsu, H.A. Viscosity data for Al₂O₃–water nanofluid—Hysteresis: Is heat transfer enhancement using nanofluids reliable? *Int. J. Therm. Sci.* **2008**, *47*, 103–111. [\[CrossRef\]](#)
20. Williams, W.; Buongiorno, J.; Hu, L.-W. Experimental Investigation of Turbulent Convective Heat Transfer and Pressure Loss of Alumina/Water and Zirconia/Water Nanoparticle Colloids (Nanofluids) in Horizontal Tubes. *J. Heat Transf.* **2008**, *130*, 042412. [\[CrossRef\]](#)
21. Chandrasekar, M.; Suresh, S.; Bose, A.C. Experimental investigations and theoretical determination of thermal conductivity and viscosity of Al₂O₃/water nanofluid. *Exp. Therm. Fluid Sci.* **2010**, *34*, 210–216. [\[CrossRef\]](#)
22. Murshed, S.M.S.; Leong, K.; Yang, C. Enhanced thermal conductivity of TiO₂–water based nanofluids. *Int. J. Therm. Sci.* **2005**, *44*, 367–373. [\[CrossRef\]](#)
23. Hamilton, R.L.; Crosser, O.K. Thermal Conductivity of Heterogeneous Two-Component Systems. *Ind. Eng. Chem. Fundam.* **1962**, *1*, 187–191. [\[CrossRef\]](#)
24. Bruggeman, D.A.G. Berechnung verschiedener physikalischer Konstanten von heterogenen Substanzen. I. Dielektrizitätskonstanten und Leitfähigkeiten der Mischkörper aus isotropen Substanzen. *Ann. der Phys.* **1935**, *416*, 636–664. [\[CrossRef\]](#)
25. Pak, B.C.; Cho, Y.I. Hydrodynamic and Heat Transfer Study of Dispersed Fluids with Submicron Metallic Oxide Particles. *Exp. Heat Transf.* **1998**, *11*, 151–170. [\[CrossRef\]](#)
26. Batchelor, G.K. The effect of Brownian motion on the bulk stress in a suspension of spherical particles. *J. Fluid Mech.* **1977**, *83*, 97–117. [\[CrossRef\]](#)
27. Esfe, M.H.; Saedodin, S.; Wongwises, S.; Toghraie, D. An experimental study on the effect of diameter on thermal conductivity and dynamic viscosity of Fe/water nanofluids. *J. Therm. Anal. Calorim.* **2014**, *119*, 1817–1824. [\[CrossRef\]](#)
28. Yu, W.; Choi, S. The Role of Interfacial Layers in the Enhanced Thermal Conductivity of Nanofluids: A Renovated Maxwell Model. *J. Nanoparticle Res.* **2003**, *5*, 167–171. [\[CrossRef\]](#)
29. Wang, X.; Xu, X.; Choi, S.U.S. Thermal Conductivity of Nanoparticle—Fluid Mixture. *J. Thermophys. Heat Transf.* **1999**, *13*, 474–480. [\[CrossRef\]](#)
30. Esfe, M.H.; Saedodin, S. An experimental investigation and new correlation of viscosity of ZnO–EG nanofluid at various temperatures and different solid volume fractions. *Exp. Therm. Fluid Sci.* **2014**, *55*, 1–5. [\[CrossRef\]](#)
31. Godson, L.; Raja, B.; Lal, D.M.; Wongwises, S. Experimental Investigation on the Thermal Conductivity and Viscosity of Silver-Deionized Water Nanofluid. *Exp. Heat Transf.* **2010**, *23*, 317–332. [\[CrossRef\]](#)
32. Timofeeva, E.V.; Gavrilov, A.N.; McCloskey, J.M.; Tolmachev, Y.; Sprunt, S.; Lopatina, L.M.; Selinger, J.V. Thermal conductivity and particle agglomeration in alumina nanofluids: Experiment and theory. *Phys. Rev. E* **2007**, *76*, 061203. [\[CrossRef\]](#)
33. Wasp, E.J.; Kenny, J.P.; Gandhi, R.L. *Solid-Liquid Flow Slurry Pipeline Transportation*; Series on Bulk Materials Handling; Trans Tech Publications: Clausthal, Germany, 1977; ISBN 978-0-87849-016-5.

34. Brinkman, H.C. The Viscosity of Concentrated Suspensions and Solutions. *J. Chem. Phys.* **1952**, *20*, 571. [\[CrossRef\]](#)
35. Bahiraei, M.; Rahmani, R.; Yaghoobi, A.; Khodabandeh, E.; Mashayekhi, R.; Amani, M. Recent research contributions concerning use of nanofluids in heat exchangers: A critical review. *Appl. Therm. Eng.* **2018**, *133*, 137–159. [\[CrossRef\]](#)
36. Sarafraz, M.M.; Safaei, M.R.; Tian, Z.; Goodarzi, M.; Filho, E.P.B.; Arjomandi, M. Thermal Assessment of Nano-Particulate Graphene-Water/Ethylene Glycol (WEG 60:40) Nano-Suspension in a Compact Heat Exchanger. *Energies* **2019**, *12*, 1929. [\[CrossRef\]](#)
37. Hassanpour, M.; Vaferi, B.; Masoumi, M.E. Estimation of pool boiling heat transfer coefficient of alumina water-based nanofluids by various artificial intelligence (AI) approaches. *Appl. Therm. Eng.* **2018**, *128*, 1208–1222. [\[CrossRef\]](#)
38. Genc, A.M.; Ezan, M.A.; Turgut, A. Thermal performance of a nanofluid-based flat plate solar collector: A transient numerical study. *Appl. Therm. Eng.* **2018**, *130*, 395–407. [\[CrossRef\]](#)
39. Elcioglu, E.B.; Genc, A.M.; Karadeniz, Z.; Ezan, M.A.; Turgut, A. Nanofluid figure-of-merits to assess thermal efficiency of a flat plate solar collector. *Energy Convers. Manag.* **2020**, *204*, 112292. [\[CrossRef\]](#)
40. Sarafraz, M.M.; Safaei, M.R.; Leon, A.S.; Tlili, I.; Alkanhal, T.A.; Tian, Z.; Goodarzi, M.; Arjomandi, M. Experimental Investigation on Thermal Performance of a PV/T-PCM (Photovoltaic/Thermal) System Cooling with a PCM and Nanofluid. *Energies* **2019**, *12*, 2572. [\[CrossRef\]](#)
41. Arkian, A.H.; Najafi, G.; Gorjian, S.; Loni, R.; Bellos, E.; Yusaf, T. Performance Assessment of a Solar Dryer System Using Small Parabolic Dish and Alumina/Oil Nanofluid: Simulation and Experimental Study. *Energies* **2019**, *12*, 4747. [\[CrossRef\]](#)
42. Hussain, M.I.; Kim, J.; Kim, J.-T. Nanofluid-Powered Dual-Fluid Photovoltaic/Thermal (PV/T) System: Comparative Numerical Study. *Energies* **2019**, *12*, 775. [\[CrossRef\]](#)
43. Bellos, E.; Tzivanidis, C. Optimization of a Solar-Driven Trigenation System with Nanofluid-Based Parabolic Trough Collectors. *Energies* **2017**, *10*, 848. [\[CrossRef\]](#)
44. Kang, W.; Shin, Y.; Cho, H. Economic Analysis of Flat-Plate and U-Tube Solar Collectors Using an Al₂O₃ Nanofluid. *Energies* **2017**, *10*, 1911. [\[CrossRef\]](#)
45. Çobanoğlu, N.; Karadeniz, Z.H.; Turgut, A. Carbon-based Nanofluid Applications in Solar Thermal Energy. In *Proceedings of the E3S Web of Conferences*; EDP Sciences: Les Ulis, France, 2019; Volume 111.
46. Alfaryjat, A.; Miron, L.; Pop, H.; Apostol, V.; Stefanescu, M.-F.; Dobrovicescu, A. Pop Experimental Investigation of Thermal and Pressure Performance in Computer Cooling Systems Using Different Types of Nanofluids. *Nanomaterials* **2019**, *9*, 1231. [\[CrossRef\]](#) [\[PubMed\]](#)
47. Ho, C.; Chang, C.; Yan, W.-M.; Amani, P. A combined numerical and experimental study on the forced convection of Al₂O₃-water nanofluid in a circular tube. *Int. J. Heat Mass Transf.* **2018**, *120*, 66–75. [\[CrossRef\]](#)
48. Çobanoğlu, N.; Karadeniz, Z.H.; Turgut, A. Nanofluid-Based Single-Phase Natural Circulation Loops. In *Nanofluids and Their Engineering Applications*; CRC Press: Boca Raton, FL, USA, 2019; pp. 59–76.
49. Rai, S.K.; Dutta, G. A Review of Recent Applications of Supercritical Fluid in Natural Circulation Loops for Nuclear Reactor. *Int. J. Appl. Eng. Res.* **2018**, *23*, 195–204.
50. Basu, D.N.; Bhattacharyya, S.; Das, P. A review of modern advances in analyses and applications of single-phase natural circulation loop in nuclear thermal hydraulics. *Nucl. Eng. Des.* **2014**, *280*, 326–348. [\[CrossRef\]](#)
51. D'Auria, F.; Frogheri, M. Use of a natural circulation map for assessing PWR performance. *Nucl. Eng. Des.* **2002**, *215*, 111–126. [\[CrossRef\]](#)
52. Cherubini, M.; Giannotti, W.; Araneo, D.; D'Auria, F. Use of the Natural Circulation Flow Map for Natural Circulation Systems Evaluation. *Sci. Technol. Nucl. Install.* **2008**, *2008*, 1–7. [\[CrossRef\]](#)
53. Misale, M.; Frogheri, M.; Ruffino, P.; D'Auria, F. Steady-state and stability behavior of a single-phase natural circulation loop. In *Proceedings of the 11th International Heat Transfer Conference*, Kyongju, Korea, 23–28 August 1998; pp. 385–390.
54. Mousavian, S.K.; Misale, M.; D'Auria, F.; Salehi, M.A. Transient and stability analysis in single-phase natural circulation. *Ann. Nucl. Energy* **2004**, *31*, 1177–1198. [\[CrossRef\]](#)
55. Jafari, J.; D'Auria, F.; Kazeminejad, H.; Davilu, H. Reliability evaluation of a natural circulation system. *Nucl. Eng. Des.* **2003**, *224*, 79–104. [\[CrossRef\]](#)

56. Kudariyawar, J.Y.; Srivastava, A.K.; Vaidya, A.M.; Maheshwari, N.K.; Satyamurthy, P.; Srivatsav, A.K. Computational and experimental investigation of steady state and transient characteristics of molten salt natural circulation loop. *Appl. Therm. Eng.* **2016**, *99*, 560–571. [[CrossRef](#)]
57. Aksan, N.; Choi, J., H.; Chung, Y., J.; Cleveland, J.; D'Auria, F.S.; Fil, N.; Gimenez, M., O.; Ishii, M.; Khartabil, H.; Korotaev, K. *Passive Safety Systems and Natural Circulation in Water Cooled Nuclear Power Plants*; International Atomic Energy Agency: Vienna, Austria, 2009.
58. Zhang, T.; Yan, Z.; Wang, L.; Zheng, W.; Su, Y. Comparative study on the annual performance between loop thermosyphon solar water heating system and conventional solar water heating system. *Sol. Energy* **2020**, *197*, 433–442. [[CrossRef](#)]
59. Boutriaa, A.; Rahmani, A. Thermal modeling of a basin type solar still enhanced by a natural circulation loop. *Comput. Chem. Eng.* **2017**, *101*, 31–43. [[CrossRef](#)]
60. Rahmani, A.; Boutriaa, A.; Hadeif, A. An experimental approach to improve the basin type solar still using an integrated natural circulation loop. *Energy Convers. Manag.* **2015**, *93*, 298–308. [[CrossRef](#)]
61. Michael, J.J.; Iniyar, S. Performance of copper oxide/water nanofluid in a flat plate solar water heater under natural and forced circulations. *Energy Convers. Manag.* **2015**, *95*, 160–169. [[CrossRef](#)]
62. Nayak, A.; Gartia, M.; Vijayan, P. An experimental investigation of single-phase natural circulation behavior in a rectangular loop with Al_2O_3 nanofluids. *Exp. Therm. Fluid Sci.* **2008**, *33*, 184–189. [[CrossRef](#)]
63. Thomas, S.; Sobhan, C.B. Stability and Transient Performance of Vertical Heater Vertical Cooler Natural Circulation Loops with Metal Oxide Nanoparticle Suspensions. *Heat Transf. Eng.* **2017**, *39*, 861–873. [[CrossRef](#)]
64. Bejjam, R.B.; Kumar, K.K.; Balasubramanian, K. Experimental Studies on Nanofluid-Based Rectangular Natural Circulation Loop. *J. Therm. Sci. Eng. Appl.* **2019**, *11*, 041006. [[CrossRef](#)]
65. Tlili, I.; Seyyedi, S.M.; Dogonchi, A.; Hashemi-Tilehnoee, M.; Ganji, D. Analysis of a single-phase natural circulation loop with hybrid-nanofluid. *Int. Commun. Heat Mass Transf.* **2020**, *112*, 104498. [[CrossRef](#)]
66. Nayak, A.; Gartia, M.; Vijayan, P. Thermal-hydraulic characteristics of a single-phase natural circulation loop with water and Al_2O_3 nanofluids. *Nucl. Eng. Des.* **2009**, *239*, 526–540. [[CrossRef](#)]
67. Misale, M.; Garibaldi, P.; Passos, J.; De Bitencourt, G.G. Experiments in a single-phase natural circulation mini-loop. *Exp. Therm. Fluid Sci.* **2007**, *31*, 1111–1120. [[CrossRef](#)]
68. Misale, M.; Devia, F.; Garibaldi, P. Experiments with Al_2O_3 nanofluid in a single-phase natural circulation mini-loop: Preliminary results. *Appl. Therm. Eng.* **2012**, *40*, 64–70. [[CrossRef](#)]
69. Vijayan, P. Experimental observations on the general trends of the steady state and stability behaviour of single-phase natural circulation loops. *Nucl. Eng. Des.* **2002**, *215*, 139–152. [[CrossRef](#)]
70. Turgut, A.; Doganay, S. Thermal performance of a single phase natural circulation mini loop working with nanofluid. *High Temp. High Press.* **2014**, *43*, 311–320.
71. Karadeniz, Z.H.; Doganay, S.; Turgut, A. Numerical study on nanofluid based single phase natural circulation mini loops. In *Proceedings of the CONV-14: International Symposium on Convective Heat and Mass Transfer, Kusadasi, Turkey, 8–13 June 2014*; Begell House: New York, NY, USA, 2014; p. 10.
72. Doganay, S.; Turgut, A. Enhanced effectiveness of nanofluid based natural circulation mini loop. *Appl. Therm. Eng.* **2015**, *75*, 669–676. [[CrossRef](#)]
73. Karadeniz, Z.H.; Doganay, S.; Turgut, A. Numerical study on nanofluid based single phase natural circulation mini loops: A steady 3D approach. *High Temp. High Press.* **2016**, *45*.
74. Koca, H.D.; Doganay, S.; Turgut, A. Thermal characteristics and performance of Ag-water nanofluid: Application to natural circulation loops. *Energy Convers. Manag.* **2017**, *135*, 9–20. [[CrossRef](#)]
75. Ho, C.J.; Chung, Y.N.; Lai, C.-M. Thermal performance of Al_2O_3 /water nanofluid in a natural circulation loop with a mini-channel heat sink and heat source. *Energy Convers. Manag.* **2014**, *87*, 848–858. [[CrossRef](#)]
76. Mohan, M.; Thomas, S.; Taha-Tijerina, J.; Narayanan, T.N.; Sobhan, C.B.; Ajayan, P.M. Heat Transfer Studies in Thermally Conducting and Electrically Insulating Nano-Oils in a Natural Circulation Loop. In *ASME 2013 International Mechanical Engineering Congress and Exposition*; American Society of Mechanical Engineers Digital Collection: New York, NY, USA, 2013. [[CrossRef](#)]
77. Duangthongsuk, W.; Wongwises, S. Effect of thermophysical properties models on the predicting of the convective heat transfer coefficient for low concentration nanofluid. *Int. Commun. Heat Mass Transf.* **2008**, *35*, 1320–1326. [[CrossRef](#)]

78. Duangthongsuk, W.; Wongwises, S. Comparison of the effects of measured and computed thermophysical properties of nanofluids on heat transfer performance. *Exp. Therm. Fluid Sci.* **2010**, *34*, 616–624. [\[CrossRef\]](#)
79. Yıldız, Ç.; Arıcı, M.; Karabay, H. Comparison of a theoretical and experimental thermal conductivity model on the heat transfer performance of Al_2O_3 - SiO_2 /water hybrid-nanofluid. *Int. J. Heat Mass Transf.* **2019**, *140*, 598–605. [\[CrossRef\]](#)
80. ANSYS Inc. *ANSYS CFX-Solver Theory Guide*; Release 19.1; ANSYS Inc.: Canonsburg, PA, USA, 2019.
81. Çengel, Y.A.; Cimbala, J.M. *Fluid Mechanics: Fundamentals and Applications*; McGraw-Hill series in Mechanical Engineering; McGraw-Hill Higher Education: New York, NY, USA, 2006; ISBN 9780073044651.
82. Parvin, S.; Nasrin, R.; Alim, M.A.; Hossain, N.; Chamkha, A.J. Thermal conductivity variation on natural convection flow of water–alumina nanofluid in an annulus. *Int. J. Heat Mass Transf.* **2012**, *55*, 5268–5274. [\[CrossRef\]](#)
83. Zhou, S.-Q.; Ni, R. Measurement of the specific heat capacity of water-based Al_2O_3 nanofluid. *Appl. Phys. Lett.* **2008**, *92*, 93123. [\[CrossRef\]](#)
84. Yu, W.; France, D.M.; Routbort, J.L.; Choi, S.U.S. Review and Comparison of Nanofluid Thermal Conductivity and Heat Transfer Enhancements. *Heat Transf. Eng.* **2008**, *29*, 432–460. [\[CrossRef\]](#)
85. Bourantas, G.C.; Skouras, E.D.; Loukopoulou, V.; Burganos, V. Heat transfer and natural convection of nanofluids in porous media. *Eur. J. Mech. B/Fluids* **2014**, *43*, 45–56. [\[CrossRef\]](#)
86. Misale, M.; Garibaldi, P.; Tarozzi, L.; Barozzi, G.S. Influence of thermal boundary conditions on the dynamic behaviour of a rectangular single-phase natural circulation loop. *Int. J. Heat Fluid Flow* **2011**, *32*, 413–423. [\[CrossRef\]](#)
87. Çengel, Y.A.; Ghajar, A. *Heat and Mass Transfer: A Practical Approach, SI Version*; McGraw Hill Education: New York, NY, USA, 2011.
88. Bejjam, R.B.; Kumar, K.K. Numerical investigation to study the effect of loop inclination angle on thermal performance of nanofluid-based single-phase natural circulation loop. *Int. J. Ambient. Energy* **2018**, *40*, 885–893. [\[CrossRef\]](#)
89. Bejjam, R.; Kumar, K. Numerical study on heat transfer characteristics of nanofluid based natural circulation loop. *Therm. Sci.* **2018**, *22*, 885–897. [\[CrossRef\]](#)
90. Sahu, M.; Sarkar, J. Steady-State Energetic and Exergetic Performances of Single-Phase Natural Circulation Loop with Hybrid Nanofluids. *J. Heat Transf.* **2019**, *141*, 082401. [\[CrossRef\]](#)
91. Thomas, S.; Sarun, K.K.; Sobhan, C.B. Flow Measurements in Metal Oxide-Nanoparticle Suspensions in a Rectangular Natural Circulation Loop. *Adv. Mater. Res.* **2013**, *685*, 145–149. [\[CrossRef\]](#)
92. Cheng, H.; Lei, H.; Zeng, L.; Dai, C. Experimental investigation of single-phase natural circulation in a mini-loop driven by heating and cooling fluids. *Exp. Therm. Fluid Sci.* **2019**, *103*, 182–190. [\[CrossRef\]](#)
93. Cheng, H.; Lei, H.; Zeng, L.; Dai, C. Theoretical and experimental studies of heat transfer characteristics of a single-phase natural circulation mini-loop with end heat exchangers. *Int. J. Heat Mass Transf.* **2019**, *128*, 208–216. [\[CrossRef\]](#)
94. Haddad, Z.; Abu-Nada, E.; Öztop, H.F.; Mataoui, A. Natural convection in nanofluids: Are the thermophoresis and Brownian motion effects significant in nanofluid heat transfer enhancement? *Int. J. Therm. Sci.* **2012**, *57*, 152–162. [\[CrossRef\]](#)

